Numerical Optimization of Circulation Control Airfoil at High Subsonic Speed

Tsze C. Tai*
David Taylor Naval Ship Research and Development Center, Bethesda, Maryland
and
George H. Kidwell Jr.†
NASA Ames Research Center, Moffett Field, California

A numerical procedure for optimizing the design of the circulation control airfoil for use at high subsonic speeds is presented. The procedure consists of an optimization scheme coupled with a viscous/potential flow analysis for the blowing jet. The desired airfoil is defined by a combination of three baseline shapes (cambered ellipse and cambered ellipse with drooped and spiraled trailing edges). The coefficients of these shapes are used as design variables in the optimization process. Under the constraints of lift augmentation and lift-to-drag ratios, the airfoil optimized at $M_\infty = 0.54$ and $\alpha = -2$ deg can be characterized as a cambered ellipse with a drooped trailing edge. Experimental tests support the performance improvement predicted by numerical optimization.

Nomenclature

a_j = airfoil coefficients (used as design variables)
C_c = chordwise force coefficient
C_d = drag coefficient (total)
C_ℓ = lift coefficient
C_n = normal force coefficient
C_p = pressure coefficient
C_μ = blowing momentum coefficient
c = chord length
H = boundary-layer shape factor, δ^*/θ
M = Mach number
N = number of panels
q = source strength
Re = Reynolds number
S = direction of search in the n-dimensional design space
s = arc length along airfoil surface
t = thickness
V = velocity
x,y = airfoil coordinates
Y = airfoil shape
α = angle of attack
α^* = scalar defining distance of travel
δ^* = boundary-layer displacement thickness
θ = boundary-layer momentum thickness
ρ = density

Subscripts

e = edge of boundary layer
i = ith panel
L = lower surface
sepl = separation point, lower surface
sepu = separation point, upper surface
TE = trailing edge
U = upper surface
∞ = freestream

Presented as Paper 84-2162 at AIAA 2nd Applied Aerodynamics Conference, Seattle, WA, Aug. 21-23, 1984; received Sept. 27, 1984; revision received April 21, 1985. This paper is declared a work of the U.S. Government and therefore is in the public domain.

*Senior Research Scientist, Aviation and Surface Effects Department. Associate Fellow AIAA.

**Research Aerospace Engineer, Advanced Plans and Programs Office. Member AIAA.

Introduction

THE David Taylor Naval Ship Research and Development Center (DTNSRDC) is the U.S. Navy's lead laboratory for circulation control (CC) technology development. Current programs include CC application to short takeoff wings and stopped-rotor (X-wing) aircraft as shown in Fig. 1. Airfoils chosen for these applications were developed almost exclusively by empirical means,[1-3] since no satisfactory theories existed during the early stages of development.

Recently, Dvorak and Kind[4] solved the wall jet flow over elliptical airfoils using a finite difference scheme along with the integral approach for flow regions where ordinary boundary layers prevail. This method, which was the most sophisticated of the methods available,[5] produced reasonably good lift momentum results, although a major deficiency in drag prediction still existed. The method has been coupled with an optimization scheme to provide an airfoil design capability for low-speed flight conditions.[6]

The X-wing aircraft, as conceived, will fly in the fixed-wing mode at speeds in the transonic regime. Consequently, a transonic version of the CC analysis program was developed by Dvorak and Choi.[7] In the present work, the previous optimization procedure[6] is extended to the transonic regime by coupling the new transonic analysis method of Dvorak and Choi[7] to the Vanderplaats scheme for designing CC airfoils in high subsonic flows. Special attention is given to deriving new airfoil shapes that will yield the highest lift for a given flow condition and specified constraints.

Analysis Method

A schematic of the flow about a CC airfoil is shown in Fig. 2. As opposed to the conventional airfoil, a typical CC airfoil is equipped with a blowing slot on the upper surface for energizing the flow in the viscous layer and a rounded trailing edge for deflecting the jet. High lift can be generated because of increased circulation created by the blowing jet. The flow is characterized by outer inviscid flow and inner viscous flow consisting of boundary layers, wall jet, and separation bubble.

The analysis method developed by Dvorak and Choi[7] was adopted with some minor modifications. The problem being considered is that of a viscous/potential flow interaction over a two-dimensional airfoil section with slot blowing on the upper surface. The transonic potential flow is calculated using

the Jameson two-dimensional transonic code (FL06)[8] with some modifications. In the Jameson procedure, the exterior of an airfoil is mapped onto the interior of a unit circle so that the entire flowfield can be solved in a finite domain. The equations are solved for the velocity potential with an estimated initial value of circulation; the velocity field is obtained by simply differentiating the potential. The solution procedure is similar to those for conventional airfoils, except that the Kutta condition is applied differently. For a blunt trailing edge, which is typical in a CC airfoil, the Kutta condition is satisfied by specifying the value of the total circulation around the airfoil.

The forward and aft stagnation points obtained by the potential flow solution divide the flows between the upper and lower surfaces of the airfoil. Based on the pressures obtained from the transonic flow solution, Cohen and Reshotko's integral method (as discussed by Brune and Manke[9]) is employed for calculating the laminar boundary layers downstream of the stagnation point for both upper and lower surfaces. After the transition predicted by Granville's empirical formula,[10] the turbulent boundary layers for the remaining lower surface to the separation point and the upper surface to the blowing slot are calculated using the Green lag-entrainment method.[11] At the slot, the turbulent boundary layer mixes with a wall jet of known velocity distribution. A finite difference scheme of the Crank-Nicolson type is used in solving the mixed flow. The flow proceeds around a highly curved surface with very strong adverse pressure gradients. The effect of the surface curvature downstream of the blowing slot is accounted for by including the curvature terms in the streamwise momentum equation and also by adding the normal momentum equation for the radial variation of the static pressure in the finite difference procedure. The flow eventually separates after passing the blunt trailing edge and a separation pressure is noted.

The viscous effects produced by the boundary-layer development are modeled by a source distribution along the airfoil surface. The source strength q at any junction point of a surface panel is obtained by

$$q=\frac{1}{\rho}\frac{\mathrm{d}}{\mathrm{d}s}(\rho V_e\delta^*) \tag{1}$$

where δ^* is the boundary-layer displacement thickness and s the arc length as measured along the airfoil surface. Equation (1) applies to the conventional boundary layers as well as to the wall jet. In the latter case, the product $\rho V_e\delta^*$ tends to decrease downstream of the blowing slot yielding a negative source strength, i.e., sink.

a) Circulation control wing with Coanda effect trailing edge to enhance lift.

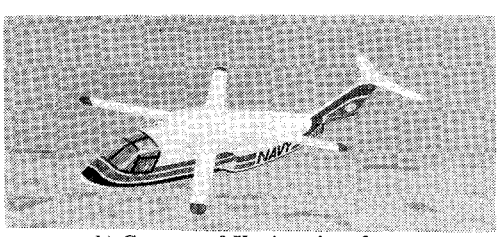

b) Concept of X-wing aircraft.

Fig. 1 Circulation control airfoil applications.

The contribution of q is then implemented in the transonic flow solution, which alters the results of the pressure distribution. The entire procedure is repeated with subsequent values of the total circulation updated. The calculations are terminated when the lift coefficient remains within a specified tolerance. At the same time, the difference in the pressure coefficients at the upper and lower ends of the separation bubble diminish. The lift coefficient is then evaluated by integrating the surface pressure distribution. The method, known as the TRACON program,[7] has been coded and written in an overlay form to reduce the core requirements.

A major difficulty in using the viscous-inviscid interaction method with the optimization code, however, is its inability to provide fairly smooth gradients of the objective function when the design variables are perturbed in the course of optimization. The problem is common in most viscous-inviscid interaction methods where the viscous and inviscid flows are calculated separately and the final solution is reached by an iterative process. To smooth out some of the irregularities in the iteratively determined pressure distribution, a second-order Lagrangian interpolation scheme is adopted for integrating the force coefficients in a similar way as in the previous work,[6]

$$C_n=\sum_{i=1}^{N+1}\left\{C_{p_i}\left(\frac{x_{i+1}-x_{i-1}}{x_i-x_{i-1}}+2\right)+C_{p_{i+1}}\left(\frac{x_i-x_{i-1}}{x_{i+1}-x_{i-1}}+2\right)-C_{p_{i-1}}\left[\frac{(x_{i+1}-x_i)^2}{(x_i-x_{i-1})(x_{i+1}-x_{i-1})}\right]\right\}\frac{(x_{i+1}-x_i)}{6} \tag{2}$$

For evaluating C_c, the x are replaced by y. The lift coefficient is

$$C_\ell=C_n\cos\alpha-C_c\sin\alpha \tag{3}$$

While the lift can be determined properly based on the integrated airfoil surface pressures, the value of the pressure drag from such an integration can yield serious errors. The source of the errors is due mainly to fluctuations in the pressure coefficient resulting from alternating viscous-inviscid calculations.[6] Therefore, the assumption that the total drag coefficient is the sum of the pressure drag and skin friction,

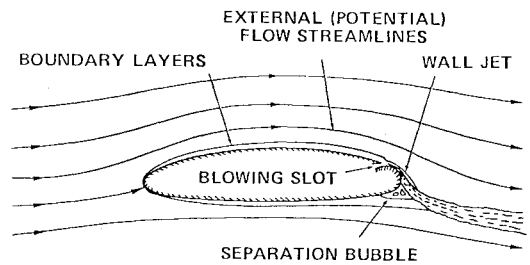

Fig. 2 Flow over a circulation control airfoil.

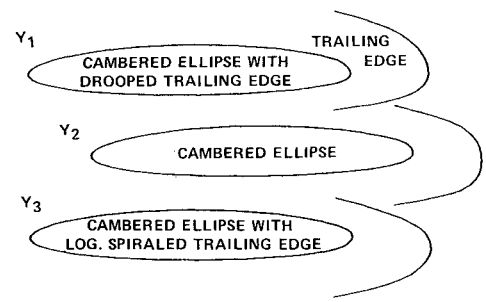

Fig. 3 Baseline shapes for airfoil representation.

less the blowing momentum coefficients, becomes inadequate. Instead, the Squire-Young method, as discussed by Smith and Cebeci,[12] has been employed for evaluating the total drag,

$$C_d = 2\left[\frac{\theta_{TE}}{c}\left(\frac{U_{TE}}{V_\infty}\right)^{H_{TE}+5/2}\right]_U + 2\left[\frac{\theta_{TE}}{c}\left(\frac{U_{TE}}{V_\infty}\right)^{H_{TE}+5/2}\right]_L \tag{4}$$

where θ_{TE} is the momentum thickness and H_{TE} is the shape factor $H_{TE} = (\delta^*/\theta)_{TE}$ at the trailing edge of the airfoil.

Optimization Procedure

Optimization Algorithm

The subject problem is to optimize the airfoil for maximum lift. Various constraints, including angle of attack, lift augmentation ratio, thickness ratio, jet detachment, and linear lift momentum flux relations can be imposed to generate optimized airfoil shapes. As with the previous work,[6] the problem is best handled by a numerical optimization scheme developed by Vanderplaats.[13]

The optimization procedure manipulates the design variables to maximize or minimize the objective subject to specified constraints. Because of the special interest in the airfoil lift capability, the present procedure will consider cases for maximizing the lift only. Therefore, for a typical case that optimizes the airfoil for maximum lift subject to thickness ratio and lift-to-drag constraints, the optimization elements are:

1) Objective to be maximized

$$C_\ell(X)$$

2) Constraints

$$(t/c)_{\min} \le t/c \le (t/c)_{\max}$$

$$(C_\ell/C_d)_{\min} \le C_\ell/C_d \le (C_\ell/C_d)_{\max} \tag{5}$$

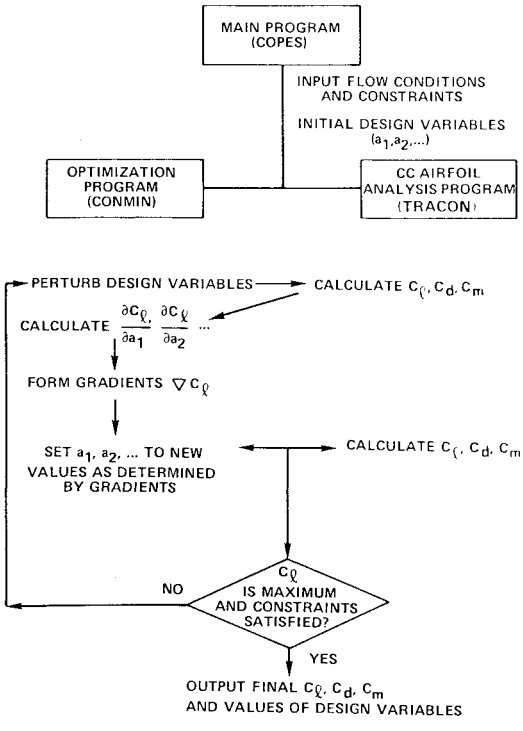

Fig. 4 Program flow chart.

3) Design variables

$$X\text{: } a_j, \quad j = 1 \cdots n$$

where a_j is the coefficient in the equation that represents the airfoil shape to be optimized. The lift coefficient C_ℓ and the drag coefficient C_d are nonlinear implicit functions of the design variables to be obtained by the analysis methods. The thickness ratio is a linear function of the design variables.

The optimization process begins with an initial X vector that is input to the program and may or may not define a feasible design. The optimization process then proceeds iteratively by the following recursive relationship:

$$X^{m+1} = X + \alpha^* S^m \tag{6}$$

The search direction S^m is obtained by initially moving in the direction of the steepest descent (the negative gradient of the objective function) without violating constraints. The scalar α^* is determined by a one-dimensional search based on a polynominal fit of several trial values. The procedure is repeated with the aid of a conjugate direction algorithm in determing the new search direction. When the constraint is encountered in the searching process, the new search direction is found using the method of Zoutendijk[14] for feasible directions. The optimum point is achieved when no direction can be found that will change the objective without violating the constraints.

Airfoil Representation

To facilitate the optimization process, the design airfoil is represented by a linear combination of n baseline profiles;

$$Y = \sum_{j=1}^{n} a_j Y_j \tag{7}$$

where Y_j represents the coordinates of a fixed baseline profile. Perturbation in coefficients a_j directly leads to changes in the resulting airfoil shape; therefore, the a_j constitute the effective design variables. While the airfoil equation (7) is general for overall airfoil shaping, the present effort is specifically to contour the blunt trailing edge because of its direct bearing on the jet deflection characteristics. Three baseline shapes (i.e., a cambered ellipse, a cambered ellipse with a drooped trailing edge, and a cambered ellipse with a logarithmically spiraled trailing edge) are employed in test cases. These shapes (shown in Fig. 3) are representative of airfoils suitable for circulation control purposes. Equation (7) thus simplifies to

$$Y = a_1 Y_1 + a_2 Y_2 + a_3 Y_3 \tag{8}$$

All three baseline shapes have identical coordinates up to $x/c = 0.95$. Variation is allowed between $0.95 \le x/c \le 1.00$. For this special case, because the thickness of the resulting airfoil remains constant, there yields

$$a_1 + a_2 + a_3 = 1 \tag{9}$$

Accordingly, Eq. (8) can be written as

$$Y = a_1 Y_1 + a_2 Y_2 + (1 - a_1 - a_2) Y_3 \tag{10}$$

The new form reduces the actual number of design variables from three to two, still with three baseline shapes. Consequently, the number of gradients has been reduced to simplify the search process. The thickness constraints, which are automatically satisfied, are also eliminated. Note that, because negative values of a_1, a_2, or a_3 are allowed, the resulting airfoil shape can be drastically different from the original profiles.

The ultimate purpose of the present work is to derive CC airfoils with improved performance for given sets of design conditions. The work involves overall airfoil shaping based on more general representation of baseline profiles. The computer program has been set up to accept as many as 25 baseline shapes, although 6 shapes would be sufficient for a broad range of interest.

Computer Program

The optimization procedure is implemented numerically by interaction between the optimization code and the airfoil analysis method. The process is shown schematically in the flow chart in Fig. 4. Specifically, the airfoil analysis program TRACON, along with an airfoil representation routine, is combined with the optimization code COPES/CONMIN. (A control program called COPES has been added to the CONMIN program by Vanderplaats,)

The program can now perform optimization runs for maximizing the lift without essential difficulty. The program requires approximately 250,000 words of core memory and 60 seconds on a CDC 7600 computer to perform one analysis calculation, with 10 iterations between the potential and viscous flows. A typical optimization run requires about 10-15 calls on the analysis program with approximately 10-15 min on a CDC 7600 computer.

Results and Discussion

Numerical results were calculated on the NASA Ames CDC 7600 computer using a remote terminal at DTNSRDC. The integrated program was first checked by the "Analysis" mode in accordance with the control options of the main program COPES before extensive "Optimization" mode runs were performed. The purpose of running the Analysis mode is to examine the accuracy of the program and to investigate the convergence of the solution procedure. The latter is of particular interest because it is known that some transonic potential flow codes may yield multivalued solutions.

Analysis runs were performed for an airfoil Model 103 at $M_\infty = 0.54$ and $\alpha = -2$ deg. A total of 66 coordinate points were used to represent the airfoil. Using the same spacing in the x coordinate, each surface of the airfoil has 33 points (or 32 panels). Special attention is then given to the proper arrangement with this limited number of coordinates. As a general rule, a relatively dense distribution in the trailing edge is required for detailed flow computations of the jet/boundary-layer mixing region. On the other hand, too sparse a coordinate distribution in other regions might lead to unrealistic results.

Typical calculated results are shown in Fig. 5. Numerical results of the lift coefficient are compared with available experimental data obtained earlier in the DTNSRDC 7×10 ft transonic wind tunnel for the same airfoil.[15] Differences exist in the trailing-edge contour and in the slot height between the experimental and numerical models: a logarithmically spiraled trailing edge and $h/c = 0.0017$ for the experimental model and an elliptic trailing edge and $h/c = 0.0014$ for the numerical model. The moderate agreement between the numerical and experimental results implies that the TRACON code is capable of rendering approximate answers for the purpose of preliminary design.

To investigate the convergence behavior of the TRACON code, a numerical exercise was carried out. Using a relatively low (estimated) initial value for the lift coefficient, the program converges consistently to a single solution. However, if the solution process is interrupted, the use of the current C_ℓ value as the initial condition for subsequent restarted iterations may converge to an answer that differs from that of a continuous "one-shot" process. It is believed that such a difference is caused by the Kutta conditions used in the program. For rounded trailing-edged airfoils, the Kutta condition is met when the pressure value as predicted by the boundary-layer calculation at the upper end of the separation bubble is equal

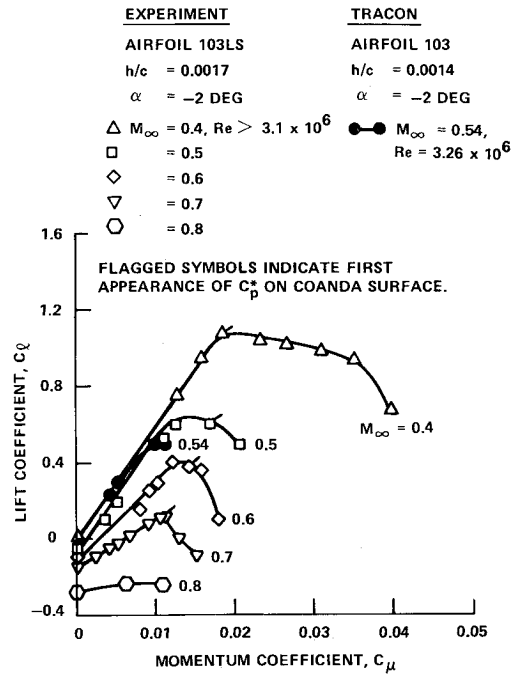

Fig. 5 Comparison of calculated results with experimental data.

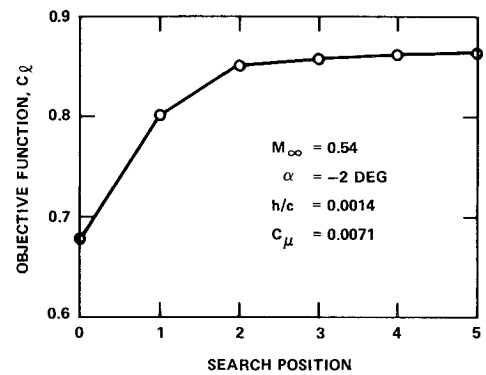

Fig. 6 Lift coefficient during the course of optimization at $M_\infty = 0.54$, $C_\mu = 0.0071$, and $\alpha = -2$ deg.

to that predicted at the lower end. Since the convergence criterion on pressure level has a tolerance of

$$|C_{p_{\text{sepu}}} - C_{p_{\text{sepl}}}| < 0.05$$

different starting conditions for overall circulation (or lift coefficient) can lead to slightly different results for integrated forces and moments. A smaller tolerance would reduce the variation with starting condition, but would greatly increase computer time and cost.

The "Optimization" results were obtained for maximizing C_ℓ with a blowing momentum coefficient C_μ of 0.0071 at Mach 0.537 and an angle of attack of -2 deg. Constraints of the lift augmentation ratio, $80 \le C_\ell/C_\mu \le 120$, and the drag-to-lift ratio, $-0.014 \le C_d/C_\ell \le 0.006$, were imposed. Analysis calculations were made for flows where the boundary layers were artificially tripped to turbulent on both surfaces of the airfoil. Figure 6 shows the value of C_ℓ vs the search position during the course of optimization. The search starts with $a_1 = 1.0$, $a_2 = 0$, and $a_3 = 0$, which yields $C_\ell = 0.678$. The search stops after the change of the objective function within a specified tolerance consecutively for five times. A final lift coefficient of 0.863 is achieved with design variables $a_1 = 1.361$, $a_2 = 0.2362$, and $a_3 = -0.5972$. The values of the

design variables that correspond to each search position are depicted in the two-variable design space in Fig. 7.

The resulting airfoil profile is shown in Fig. 8. Predominantly of baseline shape Y_1 with partial contribution of baseline shape Y_2, the airfoil can be characterized as a cambered ellipse with drooped trailing edge. The exact coordinates of the optimized airfoil are given in Table 1. The design deviates from the logarithmically spiraled trailing edge as implied by a negative value of a_3. A similar trend was found in the previous work on low subsonic cases, but to a much lesser degree. In Fig. 8, the optimized airfoil is compared with the baseline shape Y_2, which is also known as CC model NCCR 1510-7067N used in the tip section of a Kaman CC rotor. For convenience, the latter is designated the original airfoil.

To examine the off-design performance of the optimized airfoil, both numerical and experimental evaluations on the lift characteristics were carried out. Calculated data for lift coefficient vs momentum coefficient at $M_\infty = 0.54$ and $\alpha = -2$ deg are presented in Fig. 9. Using TRACON as the evaluation tool, the superior performance displayed by the optimized airfoil is of no surprise. However, the maximum value of the lift coefficient must be limited by an empirical condition such that the lift will no longer increase after the first appearance of a sonic point on the Coanda surface (after the blowing slot).[15] Therefore, the $C_{\ell_{max}}$ of the optimized airfoil should be 0.81, although higher values may be calculated in principle by TRACON, as shown by the broken line in Fig. 9.

Experimental Evaluation

Experimental tests of the two airfoils were carried out in the DTNSRDC 18 × 18 in. transonic/supersonic tunnel. To reduce model costs, the optimized airfoil was derived with a 1% extension in chord length of the original airfoil so that fabrication is accomplished by simply adding some material at the trailing edge of the existing model and milling to the desired profile. The chord lengths are 5 in. for the original airfoil and 5.05 in. for the optimized airfoil. Based on these chord lengths, experimental Reynolds numbers were $0.99\text{-}1.62 \times 10^6$. The boundary layers are either naturally transitioned or artificially tripped to turbulent. In the latter case, the tripping grit was placed at $x/c = 0.75$ on the upper surface and 0.15 on the lower surface.

Measured data of the lift coefficient vs the momentum coefficient are shown in Fig. 10. The data are chosen with test conditions that are closest to the design condition of the optimized airfoil. In general, the experiment favorably supports the improvements made by numerical optimization. Particular attention is given to the case of $M_\infty = 0.5$ where the experimental curves exhibit the predicted pattern of Fig. 9. However, the level of improvement in C_ℓ does not quite reach the earlier predictions, due to the different types of boundary layers involved. The data for the original airfoil shown in Fig. 10 are for naturally transitioned boundary layers only. The type of boundary layer seems to have little effect on the measured lift coefficients for the optimized airfoil. Unfortunately, the test data for the original airfoil with artificially tripped boundary layers are not useful because of possible experimental errors and, therefore, are not presented.

Table 1 Coordinates for optimized airfoil

N	x/c	$(y/c)_L$	$(y/c)_U$
1	0.00000	0.00000	0.00000
2	0.00069	−0.00347	0.00455
3	0.00294	−0.00724	0.00880
4	0.00731	−0.01200	0.01357
5	0.01362	−0.01667	0.01850
6	0.02923	−0.02393	0.02699
7	0.05114	−0.03098	0.03559
8	0.07303	−0.03628	0.04237
9	0.10916	−0.04295	0.05131
10	0.14529	−0.04806	0.05849
11	0.19204	−0.05317	0.06597
12	0.23879	−0.05707	0.07193
13	0.28555	−0.06007	0.07665
14	0.33369	−0.06241	0.08042
15	0.39119	−0.06434	0.08359
16	0.44871	−0.06546	0.08547
17	0.51620	−0.06582	0.08607
18	0.58550	−0.06513	0.08491
19	0.65446	−0.06334	0.08194
20	0.71939	−0.06050	0.07734
21	0.77948	−0.05666	0.07129
22	0.83131	−0.05213	0.06442
23	0.87373	−0.04726	0.05734
24	0.90725	−0.04240	0.05050
25	0.93185	−0.03900	0.04450
26	0.94688	−0.03716	0.04030
27	0.96010	−0.03480	0.03599
28	0.97153	−0.03228	0.03006
29	0.98144	−0.02930	0.02242
30	0.98911	−0.02581	0.01480
31	0.99505	−0.02157	0.00581
32	0.99851	−0.01712	−0.00213
33	1.00000	−0.01030	−0.01030
a_1, a_2, a_3	1.36100	0.23620	−0.59720

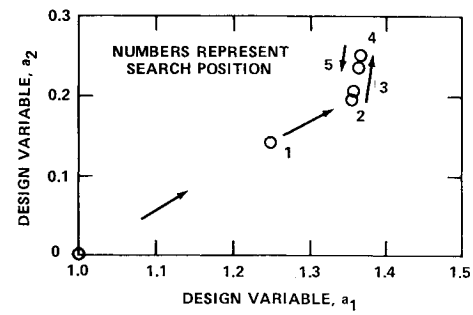

Fig. 7 Two-variable design space.

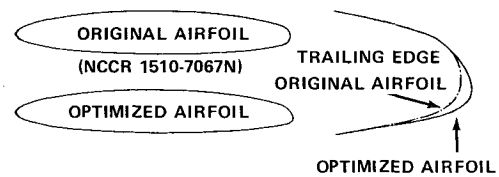

Fig. 8 Optimized airfoil based on maximizing C_L at $M_\infty = 0.54$, $C_\mu = 0.0071$, and $\alpha = -2$ deg.

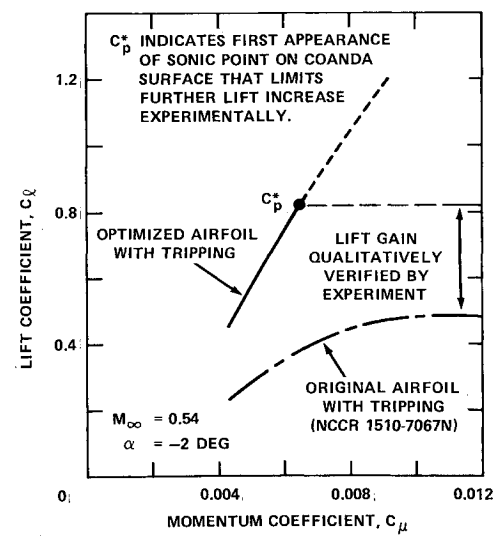

Fig. 9 Numerical off-design performance of the optimized airfoil.

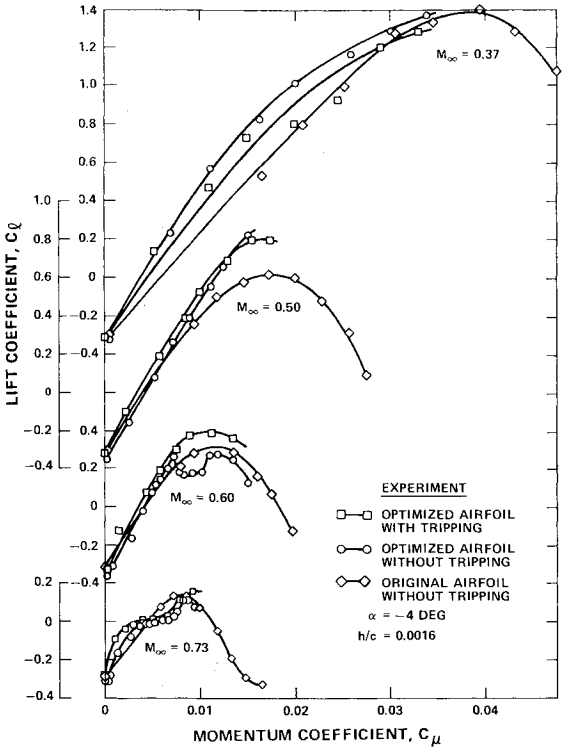

Fig. 10 Experimental off-design performance of the optimized airfoil.

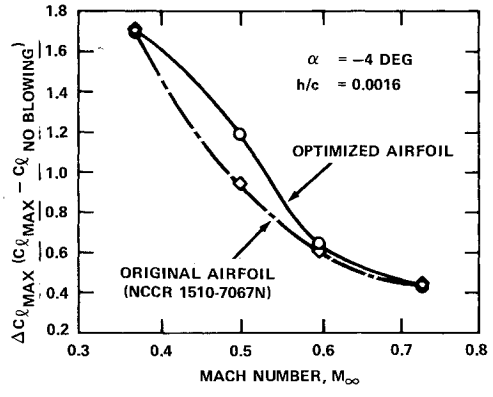

Fig. 11 Increment in lift coefficient of the optimized airfoil.

To assess the increment in lift capability of both airfoils, the experimental data are plotted in $\Delta C_{\ell_{max}}$ at various freestream Mach numbers in Fig. 11. $\Delta C_{\ell_{max}}$ is defined as the maximum lift coefficient with blowing minus the lift coefficient without blowing at a given Mach number. It appears that an increase in the $\Delta C_{\ell_{max}}$ of 25% is obtained between Mach 0.45 and 0.50. Note that there are no off-design penalties of the optimized airfoil throughout the Mach range shown. However, the two curves start to cross each other at the lower end of the Mach range. The low-speed data (not shown here) indicate that the optimized airfoil yields lesser $\Delta C_{\ell_{max}}$ than the original airfoil. For low-speed flight, therefore, the airfoil would have to be optimized subject to low-speed conditions. In fact, this has been done in the previous work.[6]

Conclusions

A useful numerical procedure has been developed for optimizing the circulation control (CC) airfoil profile at high subsonic speeds. Based on the work performed, the following conclusions may be drawn:

1) A significant gain in the lift coefficients of CC airfoils may be achieved by optimizing the trailing-edge contour. It is found that the cambered ellipse airfoil with a deeply drooped blunt trailing edge yields better high-speed aerodynamic performance than does the airfoil with an elliptic or spiraled trailing edge.

2) The experimental tests favorably support the improvements predicted by numerical optimization. An increase of 25% in the maximum lift near the design condition has been demonstrated.

Acknowledgments

This work was supported by the Independent Research Program at DTNSRDC under Work Unit 1606-105. The NASA Ames Research Center provided computer support. The authors extend thanks to J. B. Wilkerson and M. J. Malia of DTNSRDC for the many useful technical discussions of the experimental evaluation and data.

References

[1]Williams, R. M. and Rogers, E. O., "Design Consideration of Circulation Controlled Rotors," American Helicopter Society Paper 603, May 1972.

[2]Englar, R. J., "Investigation Into and Application of the High Velocity Circulation Control Wall Jet for High Lift and Drag Generation on STOL Aircraft," AIAA Paper 74-502, June 1974.

[3]Williams, R. M., "Application of Circulation Control Rotor Technology to a Stopped Rotor Aircraft Design," Paper presented at the First European Rotorcraft and Powered Lift Aircraft Forum, Southampton, England, Sept. 1975.

[4]Dvorak, F. A. and Kind, R. J., "Analysis Method for Viscous Flow Over Circulation Controlled Airfoils," *Journal of Aircraft*, Vol. 16, Jan. 1979, pp. 23-28.

[5]Englar, R. J. and Applegate, C. A., "Circulation Control—A Bibliography of DTNSRDC Research and Selected Outside References (January 1969 through December 1983)," David Taylor Naval Ship Research and Development Center, Bethesda, MD, Rept. 84/052, Sept. 1984.

[6]Tai, T. C., Kidwell, G. H. Jr., and Vanderplaats, G. N., "Numerical Optimization of Circulation Control Airfoils," *Journal of Aircraft*, Vol. 19, Feb. 1982, pp. 145-150.

[7]Dvorak, F. A. and Choi, D. H., "Analysis of Circulation Controlled Airfoils in Transonic Flow," *Journal of Aircraft*, Vol. 20, April 1983, pp. 331-337.

[8]Jameson, A., "Numerical Computation of Transonic Flows with Shock Waves," *IUTAM Symposium Transsonicum II*, Springer-Verlag, 1976, pp. 384-414.

[9]Brune, G. W. and Manke, J. W., "An Improved Version of the NASA Lockheed Multi-Element Airfoil Analysis Computer Program," NASA CR-154323, March 1978, pp. 69-87.

[10]Granville, P. S., "The Calculation of Viscous Drag of Bodies of Revolution," David Taylor Model Basin, Bethesda, MD, Rept. 839, 1953.

[11]Green, J. E., Weeks, D. J., and Brooman, J. W. F., "Prediction of Turbulent Boundary Layers and Wakes in Compressible Flow by a Lag-Entrainment Method," Royal Aircraft Establishment, England, TR-52231, Dec. 1972.

[12]Smith, A. M. O. and Cebeci, T., "Remarks on Methods for Predicting Viscous Drag," AGARD-CP-124, Oct. 1974.

[13]Vanderplaats, G. N., "CONMIN—a FORTRAN Program for Constrained Function Minimization," NASA TM X-62282, Aug. 1973.

[14]Zoutendijk, G. G., *Methods of Feasible Directions*, Elsevier Publishing Co., Amsterdam, 1960.

[15]Abramson, J. and Rogers, E. O., "High-Speed Characteristics of Circulation Control Airfoils," AIAA Paper 83-0265, Jan. 1983.